World Conference on Timber Engineering Oslo 2023

EXPERIMENTAL RESEARCH ON THE SEISMIC PERFORMANCE OF WATTLE AND DAUB INFILLED CHUAN-DOU TYPE TIMBER FRAMES

Rui Xu[1], Yunyang Qi[2], Hao Huang[1,3]

ABSTRACT: In the southwest of China, the Chuan-Dou type timber structure is widely seen in traditional dwellings, temples and halls, among which the wattle and daub (W&D) infilled wall is a relatively common embedded wall. Based on a large-scale field investigation of 30 traditional wooden structures in Chongqing, this paper had conducted experimental research on the quasi-static loading test of one bare Chuan-Dou frame and two W&D infilled Chuan-Dou frames with different wall thickness. The damage characteristic, bearing capacity, stiffness, ductility and energy dissipation of each specimen were analyzed. The results had shown that, compared with bare frame, the W&D infilled frames had obvious better lateral performance; the thicker the infill wall, the higher the bearing capacity, stiffness and dissipated energy of the specimen while also the more intense the damage of the infills.

KEYWORDS: Chuan-Dou type timber frame, Wattle and daub, Seismic performance, Quasi-static

1 INTRODUCTION

Many scholars have carried out some research on the seismic performance of traditional bare timber frames, masonry or wood panel infilled timber frames [1–3]. Finite element simulation is also one of the key research directions, so as to check the failure mode of components in the test and analyse its seismic mechanism [4,5]. However, the W&D infilled timber structure (Figure 1), which is widely distributed in the southwest of China, still lacks adequate research, it is urgent to carry out relevant research to clarify the seismic characteristics of the W&D infilled Chuan-Dou timber frames.

Figure 1: *W&D infilled timber structure*

2 EXPERIMENTAL PROGRAM

2.1 DESIGN OF SPECIMEN

In order to study the effect of the embedded wattle and daub wall and the wall thickness on the properties such as lateral resistance and damage of the wood structure wall of the pierced bucket, a total of three elements were made as follows (Table 1).

Table 1: *Parameters of each specimen (Clay : Straw scraps refers to weight ratio)*

Parameters	CK-1	QH-50	QH-60
Wall Span/mm	1400	1400	1400
Brace spacing/mm	0	350	350
Wall thickness/mm	0	50	60
Clay : Straw scraps	0	130:1	130:1

The wood used in the test was southwest spruce from China, and all walls were full-scale specimens with single layer and single span. In order to fit the structure found during the actual investigation, the footing of the wooden column was floating and the bottom of the frame was in direct contact with the top of the concrete ground beam. The foot of the two wooden columns was actually the structure of the slot directly buckled at the top of the foot. The detailed structural parameters of the standard specimen (QH-50) and the dimensions of the beam and column elements are shown in Figure 2. The size of the pure frame is the same as that of the standard specimen except that there is no embedded wall.

[1] Rui Xu, School of Civil Engineering, Chongqing University, Chongqing 400045, China, 291559092@qq.com
[2] Yunyang Qi, School of Civil Engineering, Chongqing University, Chongqing 400045, China, 2585549565@qq.com
[3] Hao Huang, Key Laboratory of New Technology for Construction of Cities in Mountain Area (Chongqing University), Ministry of Education, Chongqing 400045, China, huanghao@cqu.edu.cn

https://doi.org/10.52202/069179-0278

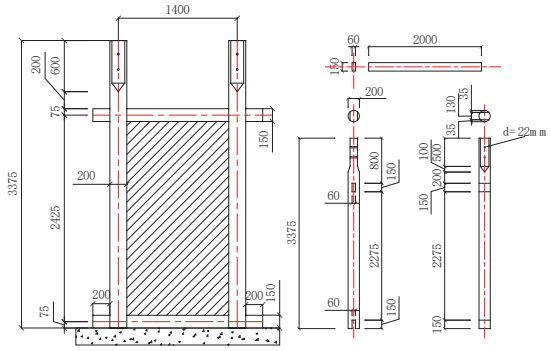

Figure 2: *Dimensions of standard specimen*

2.2 TEST SETUP AND LOADING PROTOCOL

The vertical load of the column is applied by the traditional method of hanging weights which are reinforced concrete columns for about 450kg each. It was decided to hang the weight in front of and behind each wooden column. The weights were lifted after the specimen and sensors were installed, and two weights of a column were lifted simultaneously to avoid a large out-of-plane tilt of the wall. The schematic diagram of the test piece after the overall installation is shown in Figure 3. The loading rate is also controlled at 25mm/min, and the wall cracks were plotted after all the single-cycle loading was finished and each three-cycle loading.

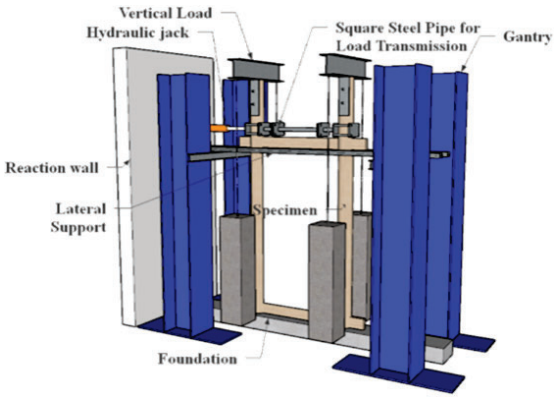

Figure 3: *Test model*

The design of the loading history referred to the international general standard, and the load-displacement curve of the static loading test of the corresponding wall is used to determine the control displacement of the structure under quasi-static loading. Finally, the loading history of pure frame and timber frame with embedded wall is determined as shown in Figure 4.

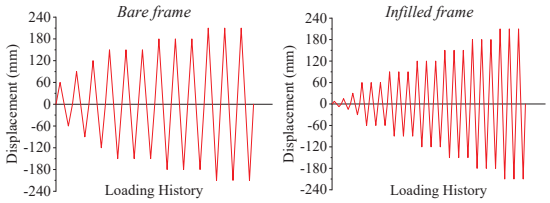

Figure 4: *Loading history*

For the unit wall of the traditional Chuan-Dou timber frame, the main horizontal displacement measurement is concentrated at the bottom of the frame and the load application site, and the vertical displacement is concentrated at the two column bases. In addition, the rotation angle and strain of each joint also need to be measured which is realized in this test with a pair of displacement gauges and strain gauges, respectively (Figure 5).

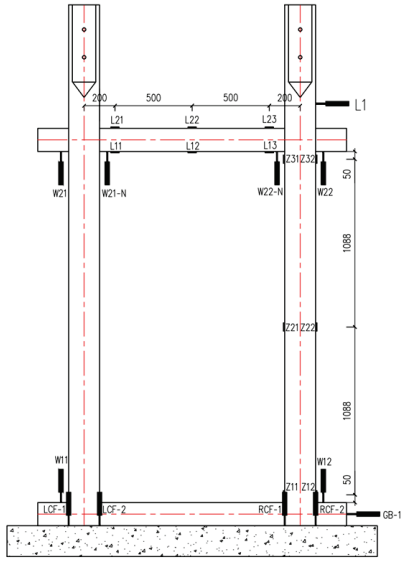

Figure 5: *Gauge arrangement*

3 TEST PHENOMENON

The embedded wall of the specimen is composed of wattle and daub and was finally finished in the form of putty smearing the surface layer. Therefore, there would be initial cracks caused by dry shrinkage cracking of the mud and specimen hoisting before the formal test. The main failure modes of the specimens are concentrated on the peeling off of the surface putty, the large area of the mud falling off, the bareness of the bamboo strips and the embedded wall separated from the frame. However, due to the variation in embedded wall and its thickness, there are differences in the stages of damage formation. The important failure process and the loading stage of each specimen are given in Table 2-4, and the crack development state and the specific failure mode are shown in Figure 6.

https://doi.org/10.52202/069179-0278

Table 2: *Summary of key experimental phenomena of specimen CK-1*

Loading stage	Key phenomena
150mm	The left and right column bases have unequal slip relative to the initial position
Third cycle of 180mm	The force transmission square steel pipe is partially pressed on the top surface of the wooden beam due to the loosening of the screw
First cycle of 210mm	The force transmission square steel pipe is all pressed on the top surface of the wooden beam. The steel parts rub violently against the wood
Second cycle of 210mm	The hysteresis curve does not show the load displacement path correctly and the test is terminated

Table 3: *Summary of key experimental phenomena of specimen QH-50*

Loading stage	Key phenomena
Before the test	Front surface fine cracks are distributed in the upper and lower part of the wall. Reverse surface cracks are spread all over the wall.
7.5-60mm	The new cracks continue to expand. The back putty is partially peeled. Some of the mud at the joints connected to the side of the column is stripped off.
120mm	When one side of the wall is pressed, the embedded wall is separated from the frame on the other side.
150-210mm	The shedding of mud material continues to develop. The embedded bamboo strips are partially exposed.

Table 4: *Summary of key experimental phenomena of specimen QH-60*

Loading stage	Key phenomena
Before the test	The initial cracks are long and thin, and the lifting process causes the putty to peel and fall off
90mm	Putty layer peeling keeps getting worse
120mm	Delamination of local surface mud and internal mud on the wall
150-210mm	Cracks are developing and large pieces of clay material are falling off more and more

Figure 6: *Test phenomenon*

4 ANALYSIS OF TEST RESULTS

4.1 HYSTERETIC LOOPS AND ENVELOPE CURVES

The comparison between hysteresis curves and envelope curves of different components are shown in Figure7.

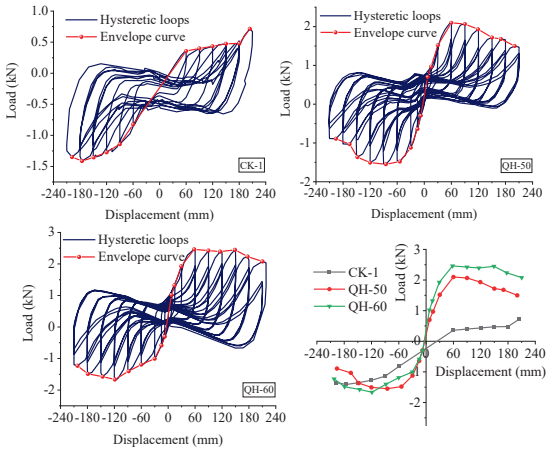

Figure 7: *Hysteretic loops and envelope curves*

Due to the initial existence of gaps in the mortise and tenon joints, the pure frame specimen showed slippage in the first loading level cycle, and the hysteresis curve showed anti-S shape. With the increase of loading level, the mortise and tenon joints exhibited more plastic deformation, and the slippage section of the hysteresis curve became longer and longer. with obvious pinching effect, the hysteresis loops of subsequent loading levels were Z-shaped. As the top force transmission square steel pipe fell on the top surface of the top beam, it was equivalent to become a part of the wall and was stressed together with the wall, so the stiffness and bearing capacity are steeply increased. It is the force transmission square steel pipe that was raised again in the back-tensioning process thus the bearing capacity began to drop at the end of the back-tensioning. It was no longer a part of the wall and the whole specimen exhibited a relatively large plastic deformation at this time which meant that the specimen began to enter yielding stage.

https://doi.org/10.52202/069179-0278

The hysteresis loops of the QH-50 specimen were shuttle-shaped at the loading level of 7.5 mm, and the load displacement was linear overall, indicating that the specimen was still in the elastic stage. With the increase of the loading level, the hysteresis loops gradually transitioned to Z-shaped, and the pinching effect became more and more obvious. The hysteresis loops of the standard specimens were obviously fuller than those of the pure frame specimens, reflecting the improvement of the energy dissipation capacity of the embedded wall with wattle and daub infill.

The development pattern of the hysteresis loop of QH-60 specimen is similar to that of QH-50, which is shuttle-shaped at 7.5 mm and Z-shaped at the subsequent large displacement loading level, and the pinching effect is intensified. The envelope curve of QH-60 specimen shows that the specimen reaches the extreme load of 2.46 kN in the positive direction at 60 mm loading level, but the obvious decrease of the load occurred after 150 mm. The drop of load before this is not significant, combined with the test phenomenon of QH-60 specimen, it can be inferred that the large area of mud shedding occurred at 180mm and afterwards caused a large discount in the bearing capacity of the specimen.

4.2 COMPARISON OF LATERAL RESISTANCE

For all loading specimens, the calculation of the lateral performance parameters is taken from the envelope curve. The calculation method is shown in Equation (1), Equation (2) and Equation (3):

$$K = \frac{0.3F_{\max}}{D_{0.4F_{\max}} - D_{0.1F_{\max}}} \tag{1}$$

$$G = \frac{F_{\max}}{2D_y} \times \frac{H}{L} \tag{2}$$

$$d = \frac{D_{\max}}{D_y} \tag{3}$$

where K = secant stiffness, F =force, D = displacement, G = shear stiffness, H = height, L = width, d = ductility.

The calculation results based on the above formula are shown in Table 5.

Table 5: *Comparison of lateral performance parameters between specimens*

Parameters	CK-1	QH-50	QH-60
K (kN/m)	9.850	55.350	88.618
G (kN/m)	10.063	102.560	171.127
d	3.41	3.47	4.79

It can be found that because there is no embedded wall, the mortise and tenon joints become the main part to resist the lateral force, and the role of the joint alone is relatively limited, so the embedded wall has a significant improvement in the bearing capacity. In terms of ductility, the two specimens (CK-1 and QH-50) also show different characteristics in the positive and negative directions. The ductility of the positive loading is similar, while the ductility of QH-50 is significantly larger than that of the pure frame. The embedded wattle and daub wall also significantly improves the initial stiffness and overall shear stiffness. In general, the bearing capacity, stiffness and ductility of the timber frame are obviously improved by the embedded wall. In terms of bearing capacity, the specimen shows that the thicker the wall, the higher the bearing capacity and the ductility of QH-60 is higher than that of QH-50 at the same time.

4.3 STIFFNESS DEGRADATION

The change in stiffness of a timber frame can reflect the magnitude of the frame's ability to resist deformation. The stiffness degradation reflects the cumulative damage to the joints of the timber frame which can be described by the secant stiffness K_i defined by Equation (4):

$$K_i = \frac{\left|+P_i\right| + \left|-P_i\right|}{\left|+\Delta_i\right| + \left|-\Delta_i\right|} \tag{4}$$

where P = peak load, Δ = displacement.

The comparison of the stiffness degradation between the wall thickness parameter specimens and the standard specimens with each other is shown in Figure 8. From the curve change, it can be found that the initial stiffness of the CK-1 specimen (l=60 mm) is 9.85 kN/m, and its stiffness decreases continuously during the loading process. Finally, it is only 4.91 kN/m which is a decrease of 50.2%.

The other two walls have much greater stiffness than the CK-1 specimen at the same loading level due to the presence of the embedded wall. Figure 8 shows that QH-60 has the largest initial stiffness of 88.13 kN/m, followed by QH-50 with 71.13 kN/m. During the subsequent loading, the stiffness of QH-60 is greater than the other two specimens from beginning to end.

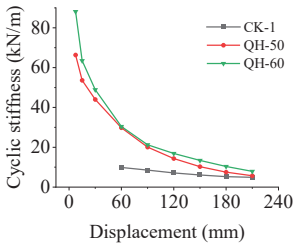

Figure 8: *Stiffness degradation*

The stiffness of all the specimens with embedded walls continuously decreased during the loading process, which was mainly caused by the accumulated plastic deformation of the mortise and tenon joints and the continuous development of the mud shedding in the walls. However, it can be found that the effect of increasing the wall thickness on improving the stiffness of the specimens is relatively obvious.

4.4 STRENGTH DEGRADATION

Strength degradation is caused by cumulative fatigue damage to structural specimens or joints, the magnitude of which determines whether the structure can maintain a good load bearing capacity under multiple cycles of lateral forces. Define R2/R1 as the ratio of the second

https://doi.org/10.52202/069179-0278

cycle peak load to the first cycle peak load at the same displacement control level, and R3/R2 as the ratio of the third cycle peak load to the second cycle peak load at the same displacement control level. These two parameters are used to quantitatively describe the strength degradation of the specimens. The R2/R1 and R3/R2 curves of all specimens are shown in Figure 9.

It can be found that the strength degradation curves of the three walls do not show an obvious rule, but the degradation occurs mainly in the second cycle. The steep increase in R3/R2 at 180 mm for CK-1 is due to the pressure of the force-transmitting square steel tube on the top surface of the top beam, which is mentioned in the test phenomenon before.

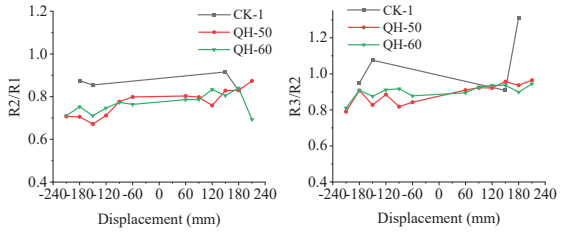

Figure 9: *Strength degradation*

4.5 ENERGY DISSIPATION

The energy dissipation ability of the structure is an important criterion to evaluate the seismic performance. The load-displacement hysteresis curve obtained by the test can calculate the energy dissipated by the structure at different loading levels, which is the area $S_{ABC} + S_{ACD}$ included in the hysteresis loop shown in Fig. 10. The energy dissipation of the structure is mainly manifested as the energy generated by the earthquake or cyclic loading is converted into heat energy or other forms of energy by the deformation and damage of the component or the whole wall.

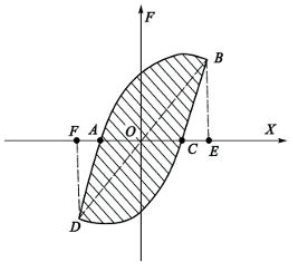

Figure 10: *The schematic diagram of the calculation of the area of hysteretic curve*

In order to better describe the energy dissipation ability of the structure, the equivalent viscous damping ratio (EVDR) is adopted as shown in Equation (5):

$$h_e = \frac{1}{2\pi} \cdot \frac{S_{ABC} + S_{ACD}}{S_{OBE} + S_{ODF}} \quad (5)$$

where h_e = EDVR, S = area.

For the specimens with different wall thickness, the energy dissipation curves and equivalent viscous damping ratio curves at each level are shown in Figure 11 and Figure 12, respectively.

.

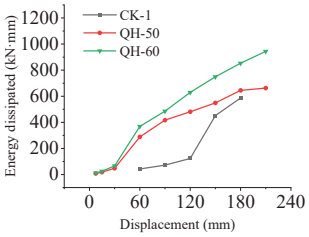

Figure 11: *The energy dissipation curve of all specimens*

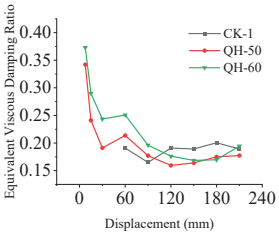

Figure 12: *Energy dissipation and equivalent viscous damping ratio (EVDR)*

It can be found that the pure frame has the lowest energy dissipation among all specimens at each loading level. When the loading displacement was small, the pure frame dissipated energy mainly through the extrusion of the mortise and tenon joints. With the loading displacement increasing, the whole specimen exhibited uncoordinated deformation due to the absence of the restraint of the embedded wall. In addition to the rotation extrusion at the joint of the pure frame specimen, the friction movement deviating from the initial position occurred and the bottom of the wall also rubbed back and forth with the surface of the floor beam during the cyclic loading process, which increased the energy dissipation of the pure frame to a certain extent, so the energy dissipation curve of the pure frame had a relatively obvious increase after 150mm loading displacement.

For both frames with embedded wall, during the whole loading process, the mud gradually dropped in blocks and the bonding between mud and the embedded bamboo strip mesh became worse. Under the large displacement loading section, the structural system cannot be formed between each other, so the energy dissipation ability decreased rapidly with the increase of displacement. In the single-cycle loading section, the energy dissipation of QH-60 was slightly higher than that of the other two specimens, but the overall difference was not significant. In the three-cycle loading section, the energy dissipation of QH-60 specimen was larger than that of QH-50. The comparison of the curves of QH-60 and QH-50 shows that the increase of wall thickness significantly improves the energy dissipation of the specimen.

The trend of the EVDR curve of the two embedded walls is similar, which is reflected in the continuous decline of the single cycle loading section. The curve has a rise when

https://doi.org/10.52202/069179-0278

entering the first three cycles, followed by a slow decline, and finally the curve has risen again. The phenomenon is related to the energy dissipation mechanism of the specimen. The small displacement loading section relied mainly on the nodal energy dissipation of the frame. With the increase of the loading stage, the hysteresis loop transformed from the shuttle shape to the longer anti-S shape of the slip section, and the energy dissipation efficiency was reduced. In the subsequent loading process, the mud wall began to have a relatively large extrusion with the wooden column, and the EVDR value of the specimen began to rise at l = 60mm due to the increase of the energy dissipation part, and the energy dissipation capacity was improved. Subsequently, the wall was damaged to varying degrees, and the EVDR value continued to decline due to the reduction of energy consuming parts. At the end of loading, friction energy dissipation began to occupy the main part, and the energy dissipation efficiency of each specimen was improved. The energy dissipation capacity of QH-60 is only slightly lower than that of QH-50 at 180 mm, while the other loading sections are higher than the standard specimen. It can be seen that the wall thickness improves the energy dissipation capacity.

The resistance of the traditional timber frame with wattle and daub infill mainly comes from the mortise and tenon joints, the mud wall itself and a large amount of frictional slip. The initial gap at the nodes and the wood joints have different effects on the lateral resistance and energy dissipation of the specimens. The main energy dissipation mechanisms of the traditional timber frame with embedded wall are shown in the following aspects. At the beginning of the test, the energy dissipation capacity decreased because the joints mainly provided resistance leading to the development of hysteresis loop pinching and shrinkage. In the middle of the test, the wall started to play more role in energy dissipation, but it decreased again with the increase of wall damage. In the later part of the test, various frictional effects had a greater impact on energy dissipation.

5 CONCLUSIONS

Based on the results of cyclic loading test, the main conclusions can be drawn as follows:

(1) Compared with bare frame, the W&D infilled frames had better bearing capacity and stiffness.
(2) The bearing capacity, stiffness and dissipated energy of W&D infilled frames can be obviously improved by increasing the wall thickness.

ACKNOWLEDGEMENT

This work was financially supported by the National Natural Science Foundation of China (grant no. 51978102).

REFERENCES

[1] Hao H., Yuntian W., Zhao L., et al.: Seismic behavior of Chuan-Dou type timber frames. Engineering Structures, 167:725-739, 2018.
[2] Zhe Q., Xiang F., Shoichi K., et al.: Behavior of masonry infilled Chuandou timber frames subjected to in-plane cyclic loading. Engineering Structures, 211:110449, 2020.
[3] Emile C., Xiaobin S., Yajie W., et al.: Lateral performance of mortise-tenon jointed traditional timber frames with wood panel infill. Engineering Structures, 161: 223-230, 2018.
[4] LI S. Behavior of traditional Chinese mortise-tenon joints: Experimental and numerical insight for coupled vertical and reversed cyclic horizontal loads[J]. Journal of Building Engineering, 2020: 15.
[5] YANG Q. Load resisting mechanism of the mortise-tenon connection with gaps under in-plane forces and moments[J]. Engineering Structures, 2020: 16.

https://doi.org/10.52202/069179-0278